

Supplementary Materials

Contents of this file:

Figures S1 to S16

Tables S1 to S6

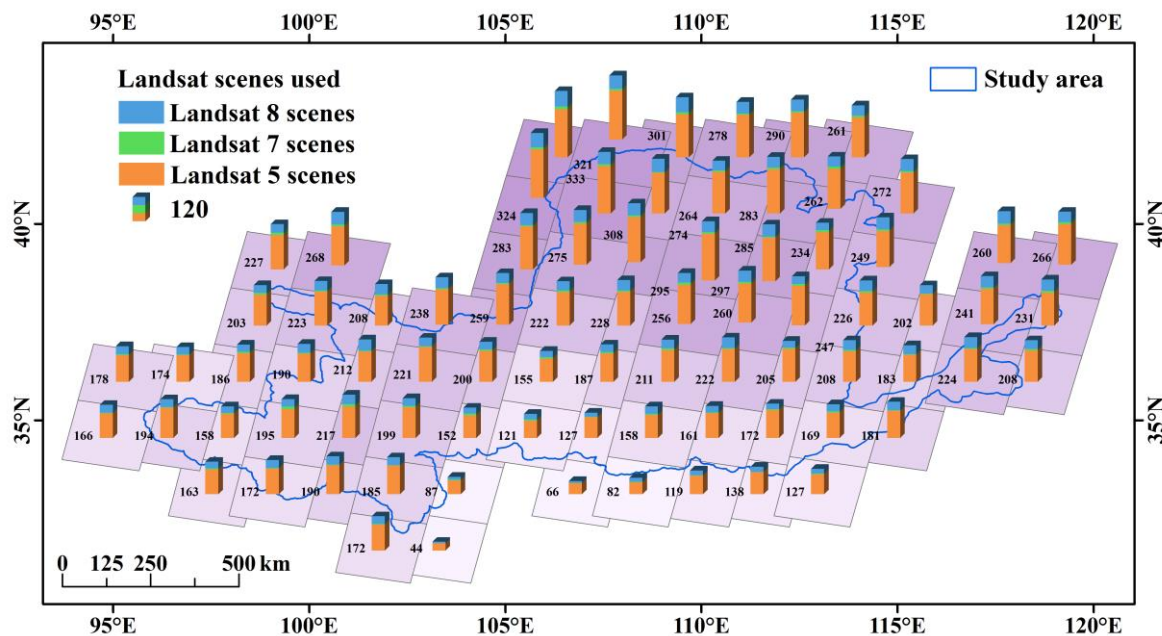


Figure S1. Geographical distribution of Landsat scenes used.

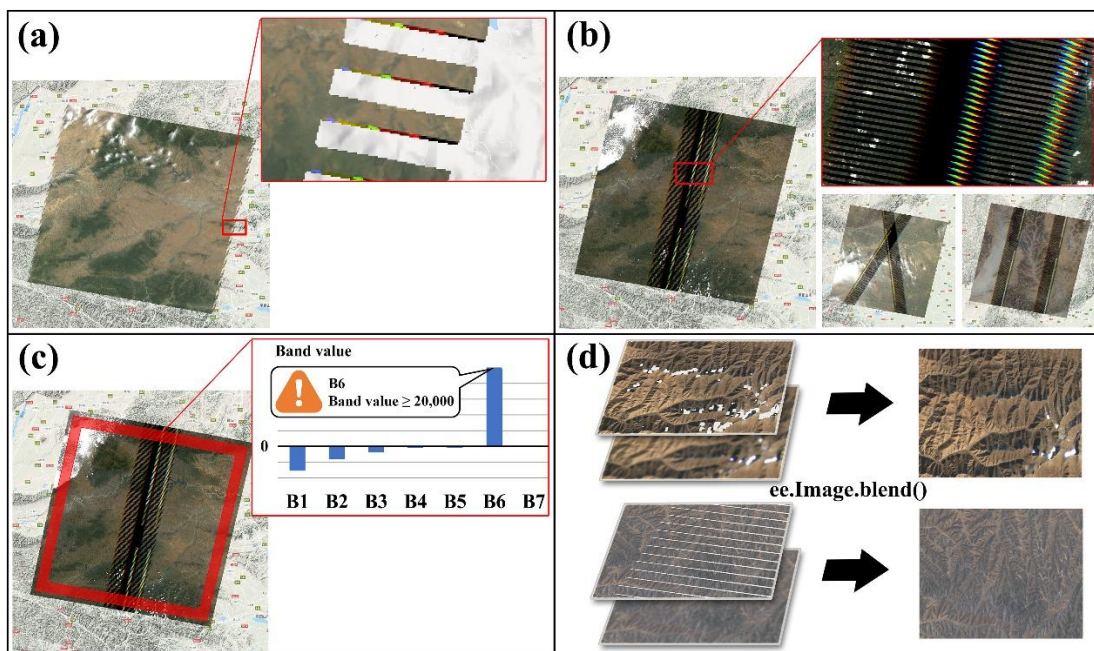


Figure S2. (a) Christmas tree anomaly. (b) Caterpillar tracks run throughout the whole image scene. (c) Statistically monitor the annulus area to identify the scene which has caterpillar tracks. The purpose of using annulus instead of rectangular bounds of image scene is to save GEE user memory. (d) The gap filling of missing data and Landsat 7 gaps.

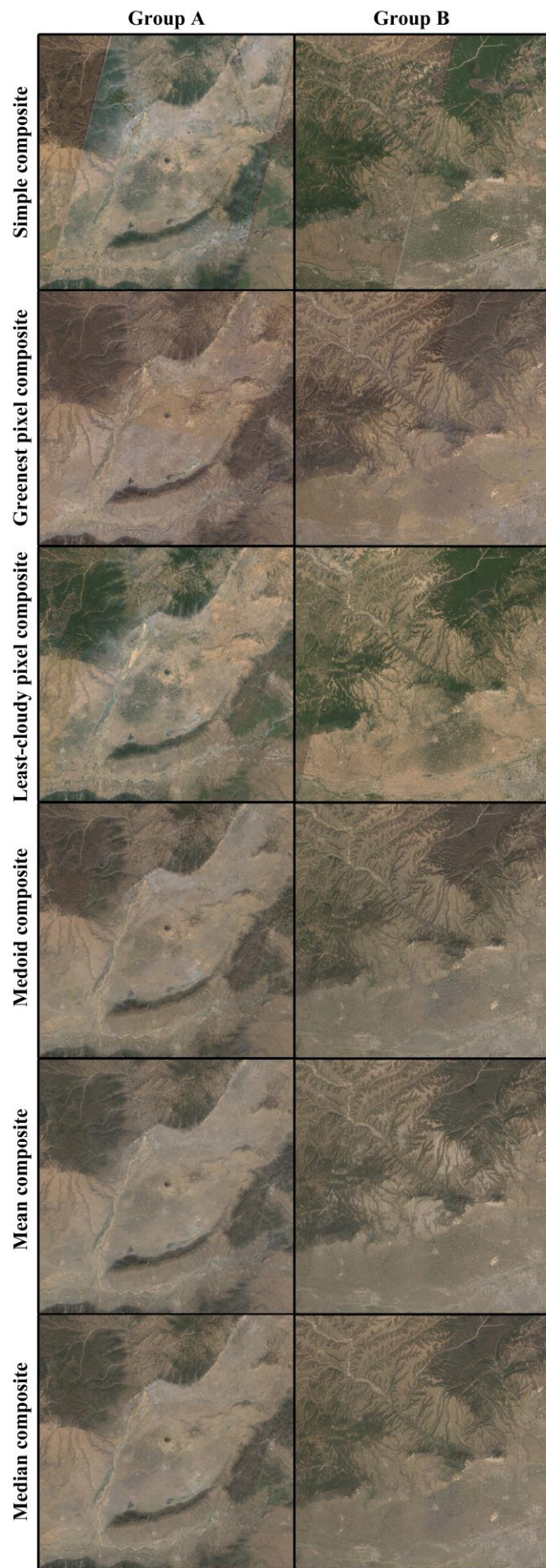


Figure S3. Comparison of 6 composite methods image effects achieved in GEE on two areas.

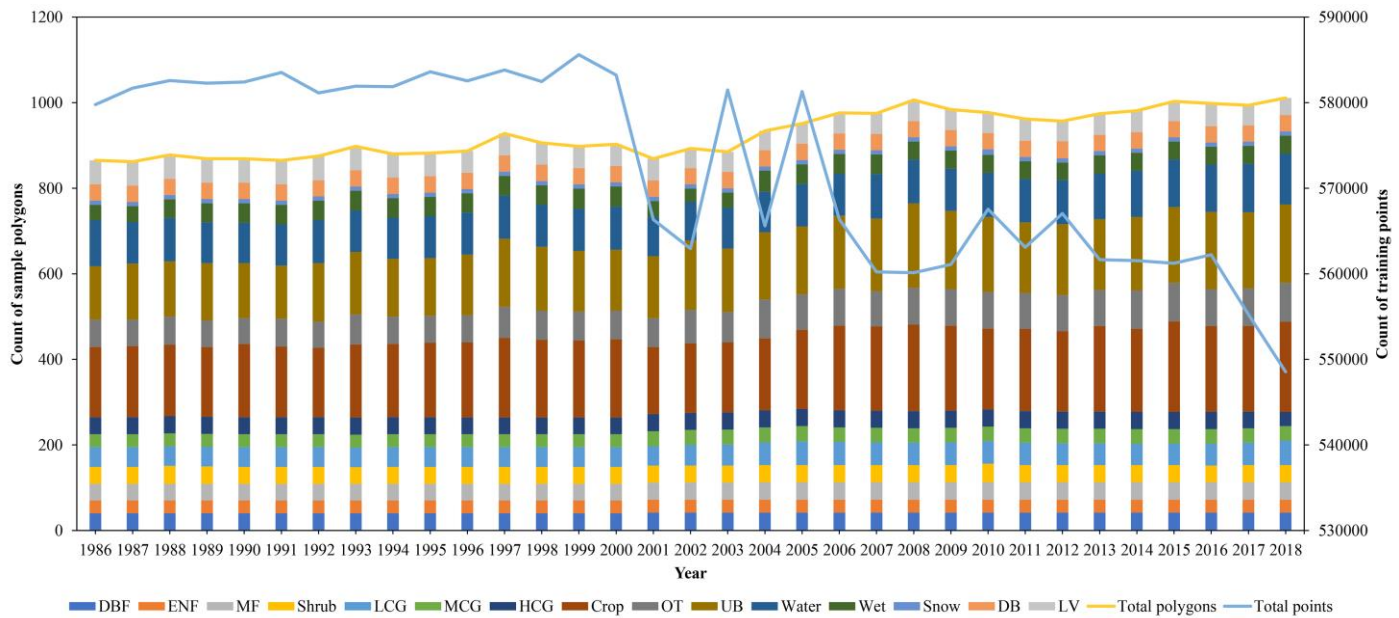


Figure S4. The distribution of training sample polygons in time and class.

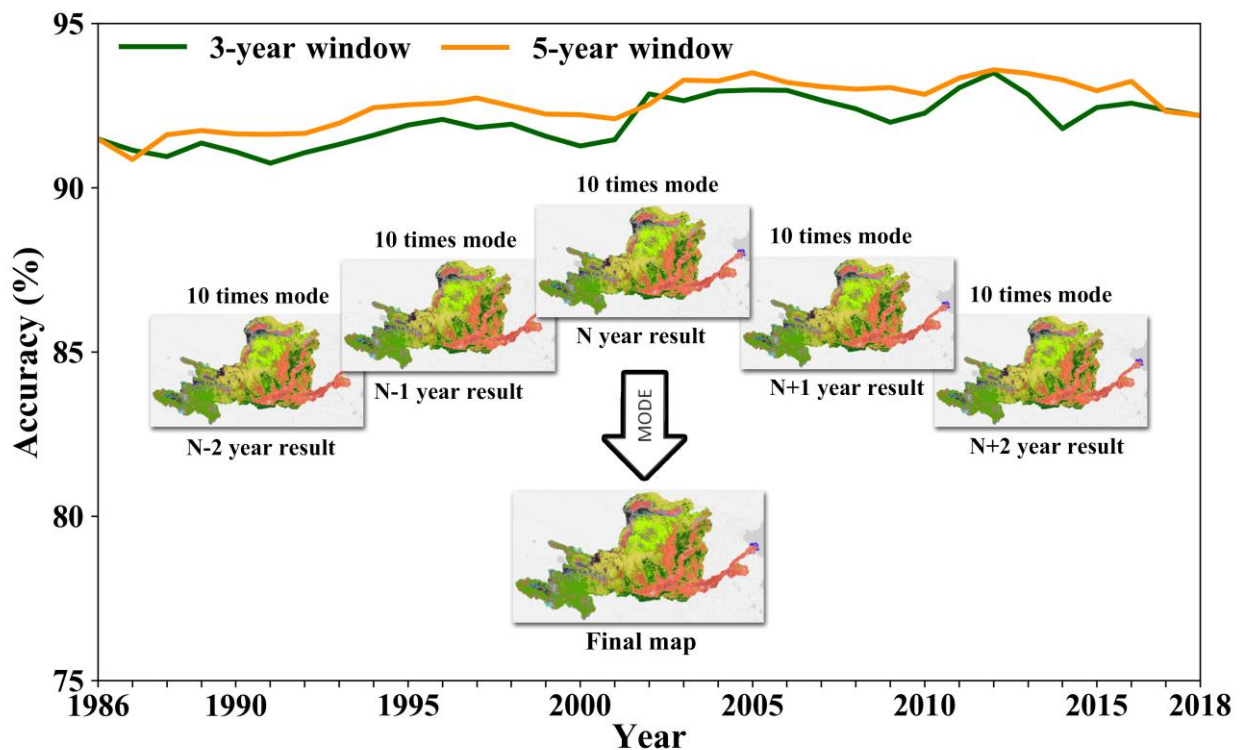


Figure S5. Moving the sliding window to adjust temporal consistency and the accuracy is calculated by reference samples in each year.

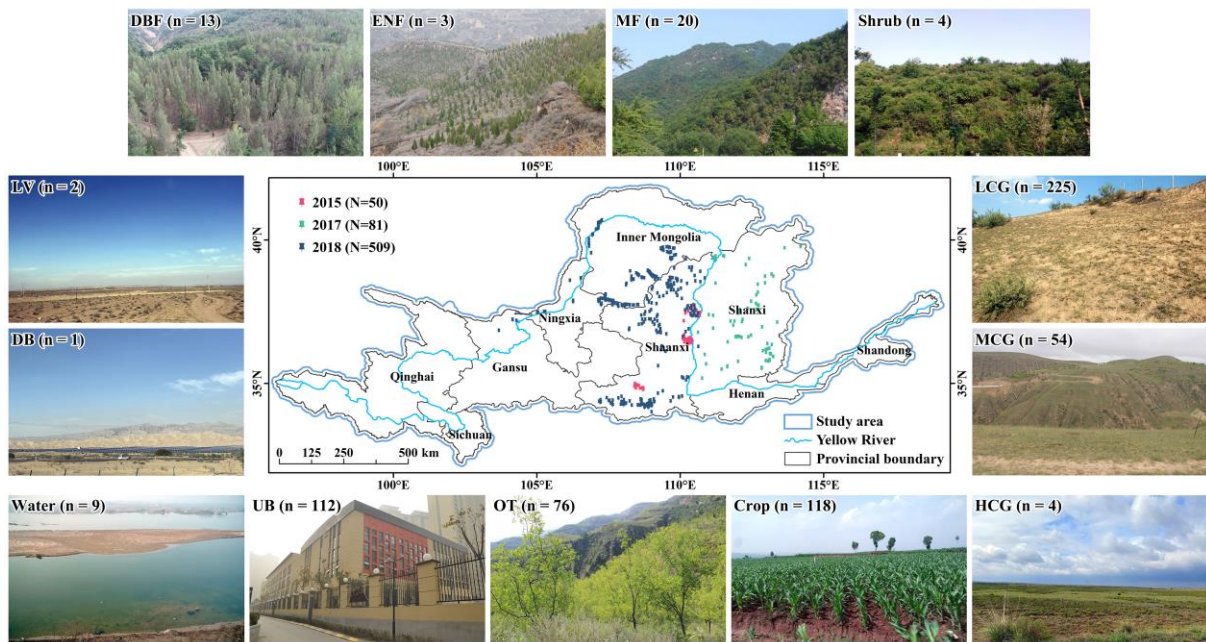


Figure S6. The geographical distribution of ground points for validation. These points were collected during the field survey in 2015, 2017, and 2018 within the Yellow River basin. Insets are the illustration of some points.

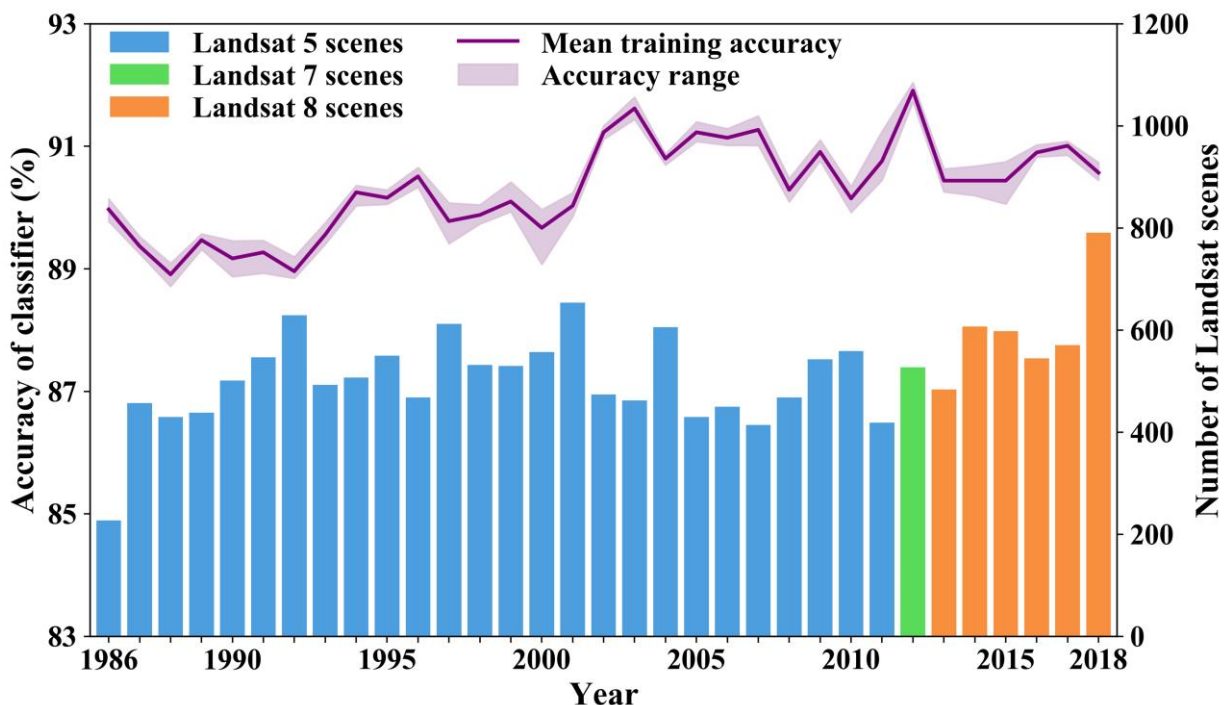


Figure S7. Training accuracy of classifiers and the number of Landsat scenes used in each year. The accuracy range is determined by the maximum and minimum value of 10 times classifications in each year.

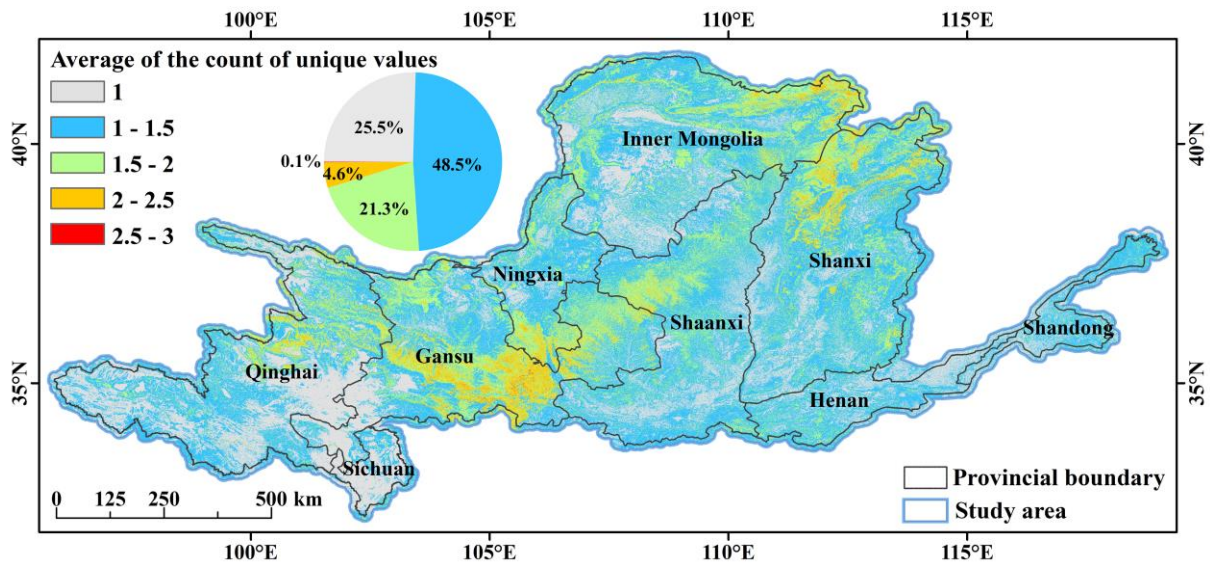


Figure S8. Average of the count of unique values in 10 classifications for each pixel each year for 33 years. The classifiers are more stable in areas with smaller values.

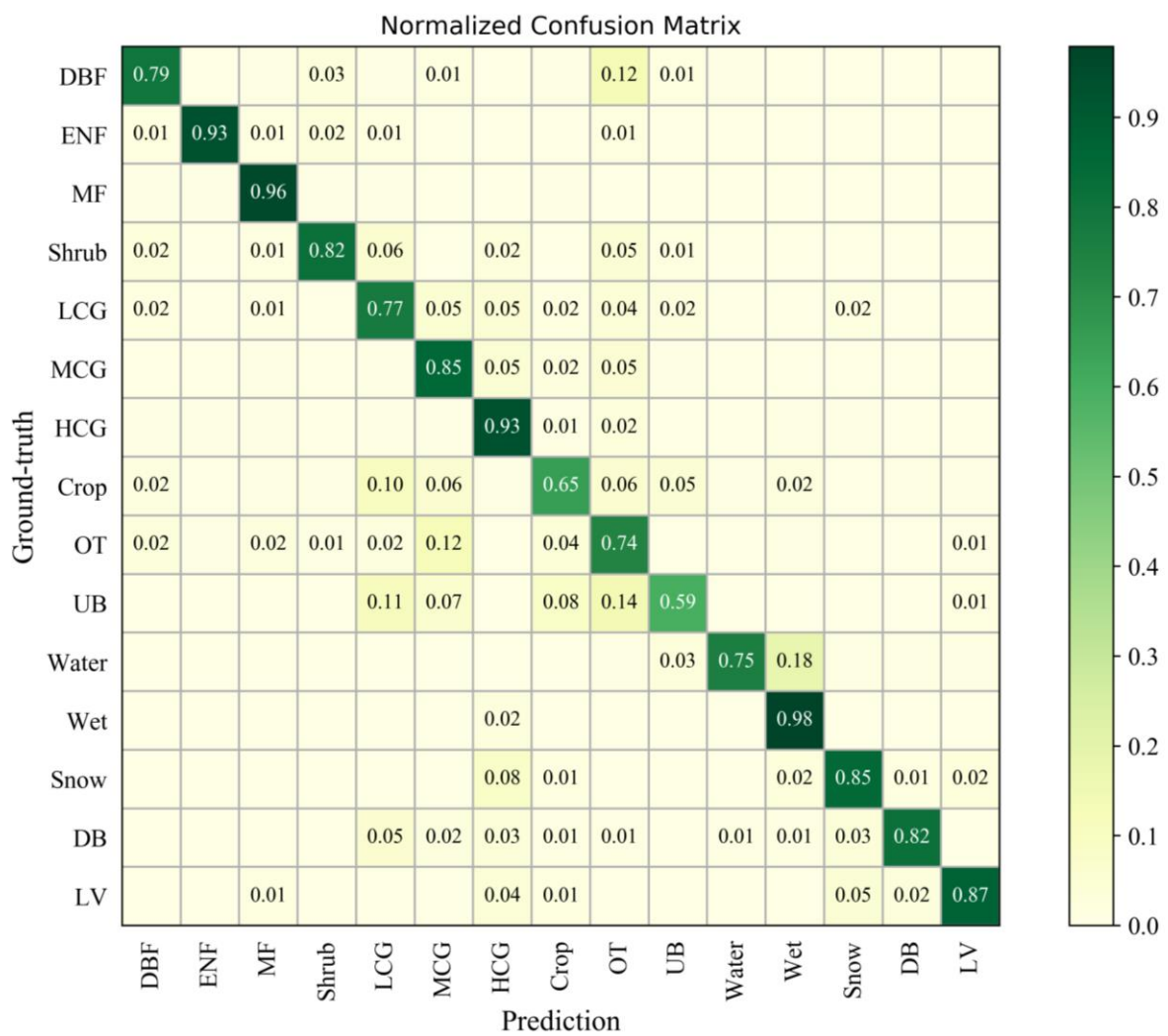


Figure S9. Normalized confusion matrix of 3456 independent stratified random sampling validation points set from 2001 to 2018.

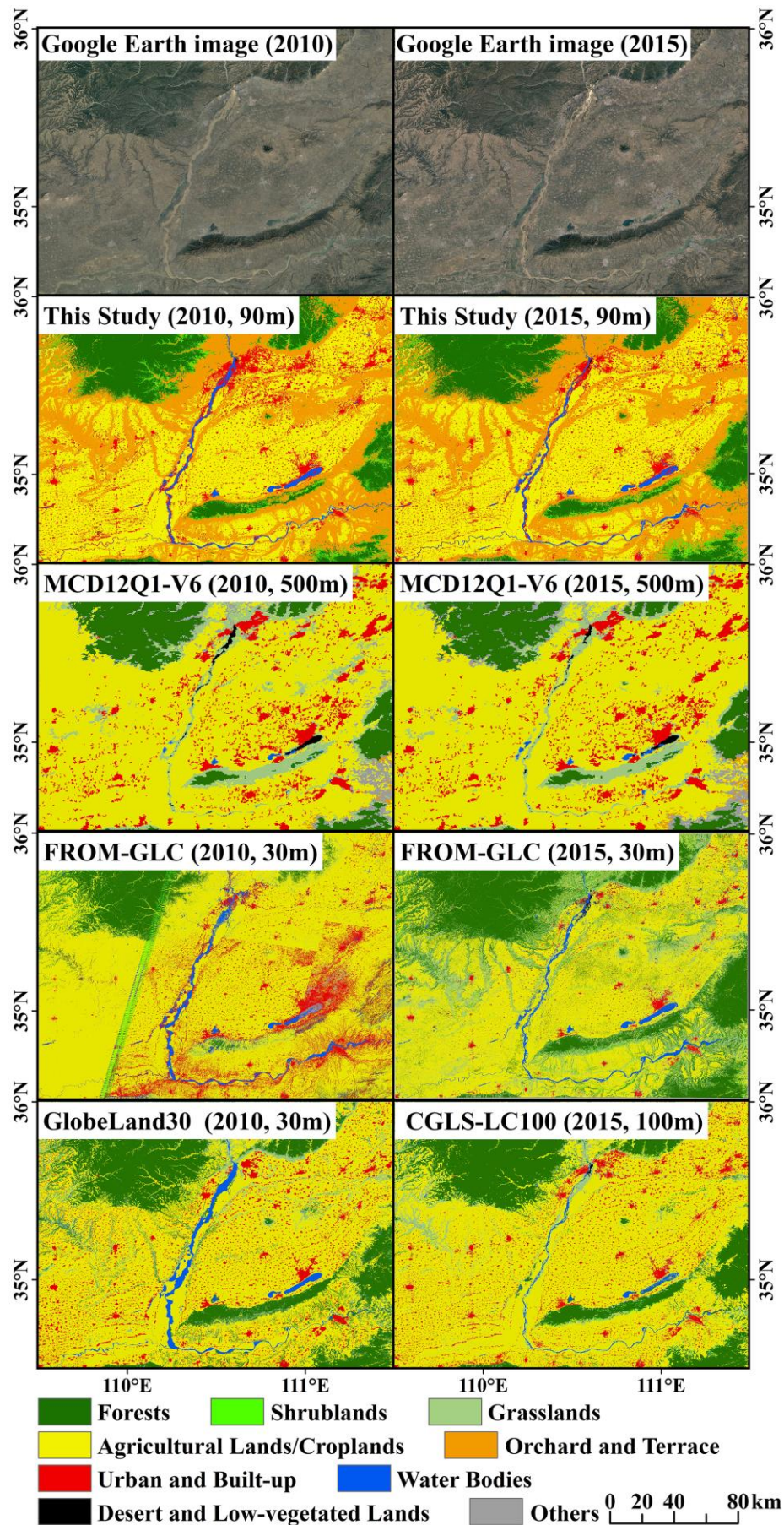


Figure S10. Comparison of different land use/cover datasets within a region in the middle reaches of the Yellow River in 2010 and 2015. The data of this study divides agricultural lands into croplands and orchard and terrace classes.

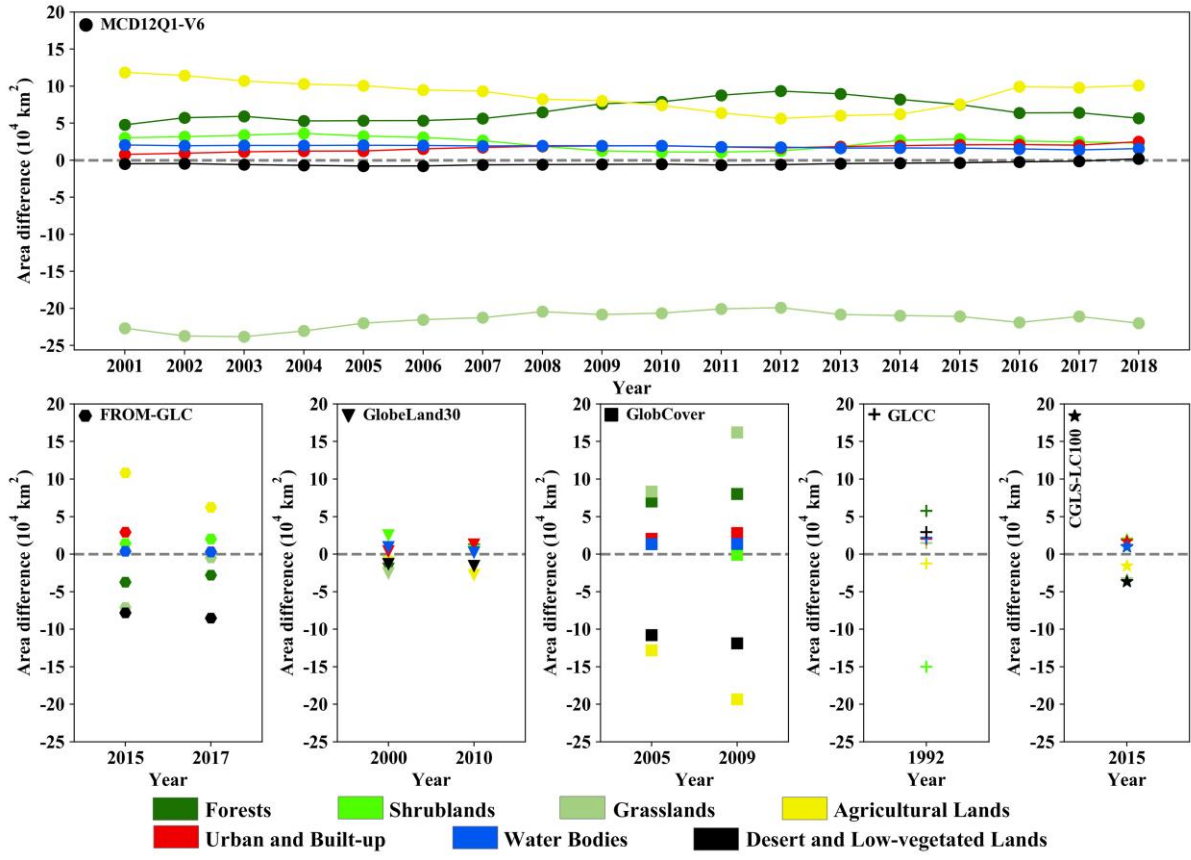


Figure S11. The difference in area between other land use/cover products and this study in the first-degree classes (this study - other product).

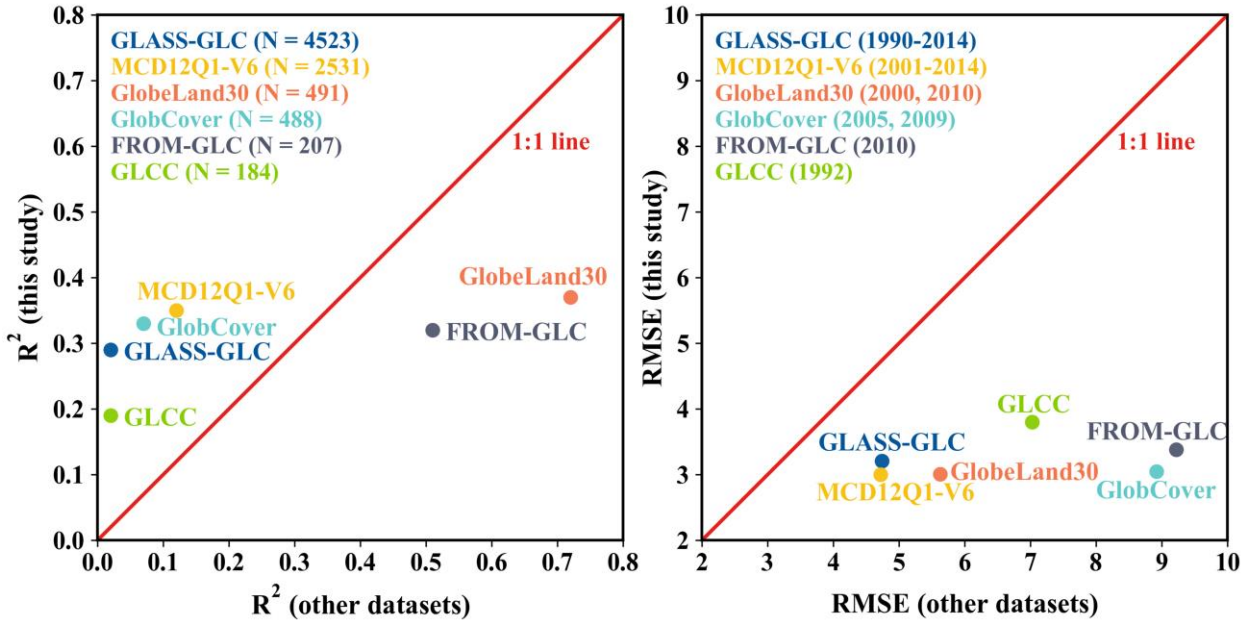


Figure S12. Comparisons between the estimated croplands areas in each product and those obtained from the statistical dataset in different time periods.

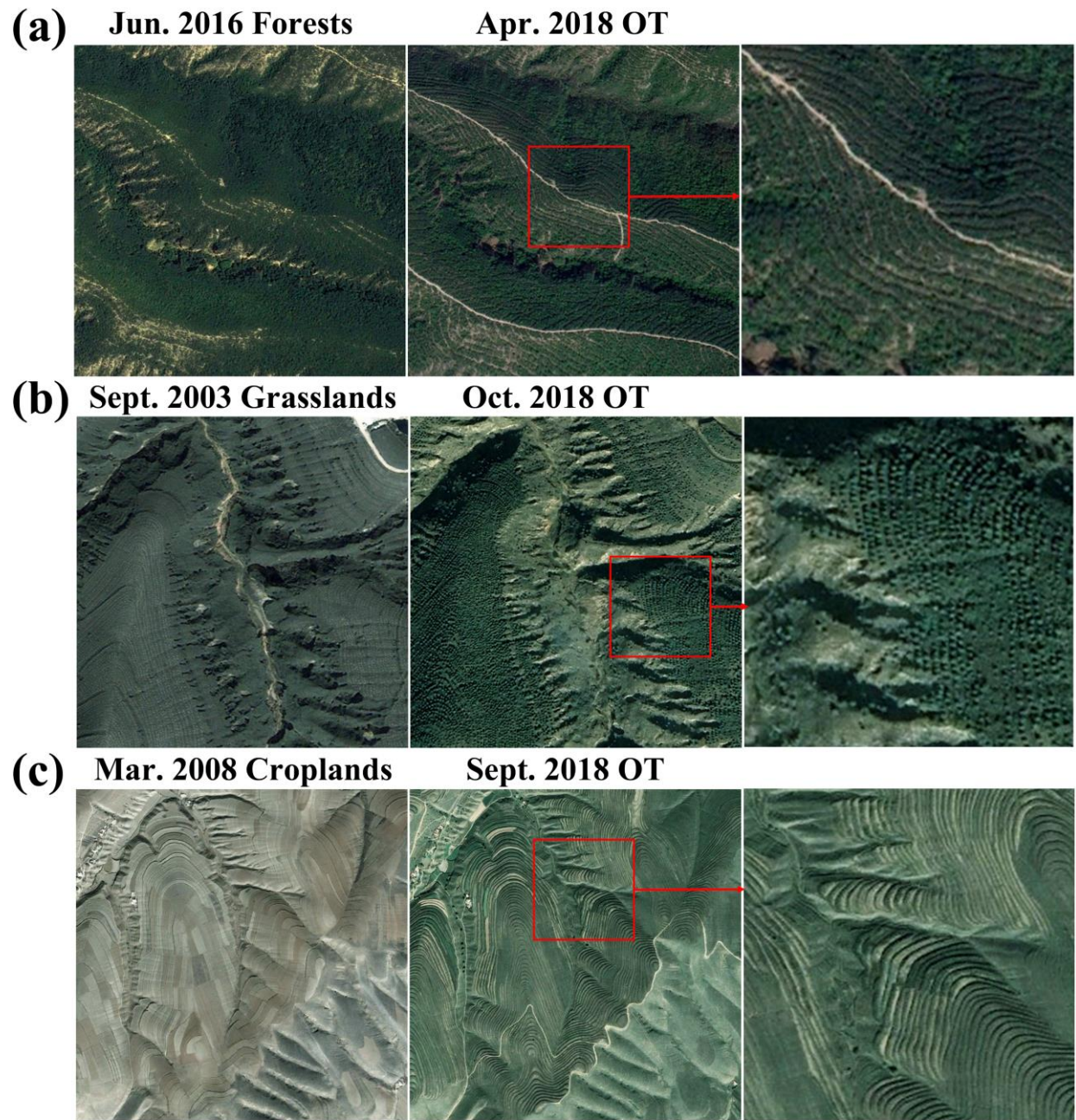


Figure S13. Examples of the transition of forests (a), grasslands (b), and croplands (c) to orchard and terrace (OT) on Google Earth images, respectively.

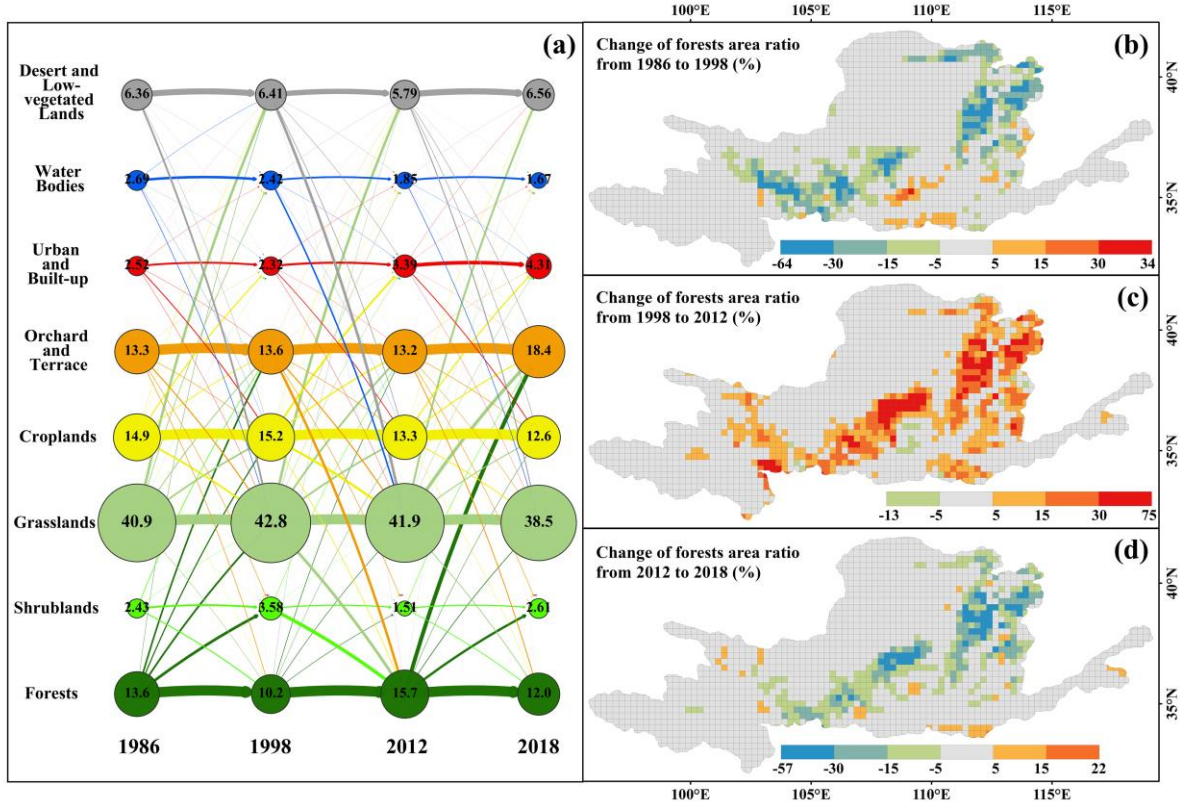


Figure S14. Change in forests from 1986 to 2018. (a) Land use/cover transition network of all the pixels in the study area for different periods. The numbers within the cycles in the figure is the area (10^4 km^2) of each class in the corresponding year. Geographical distribution of the change of forests area ratio during (b) 1986-1998, (c) 1998-2012, and (d) 2012-2018 in the Yellow River basin. The change in area ratio was obtained in each grid (0.5°).

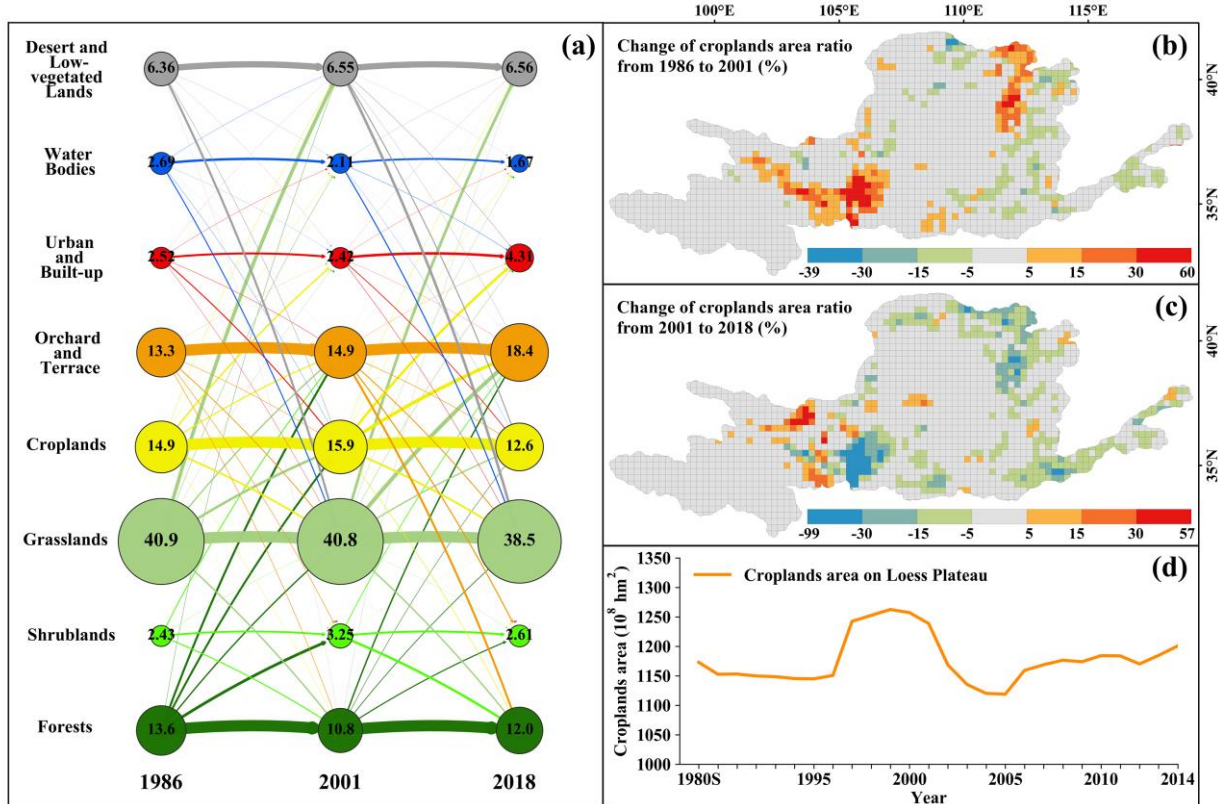


Figure S15. Change in croplands from 1986 to 2018. (a) Land use/cover transition network of all the pixels in the study area for different periods. The numbers within the cycles in the figure is the area (10^4 km^2) of each class in the corresponding year. Geographical distribution of the change of croplands area ratio during (b) 1986-2001 and (c) 2001-2018 in the Yellow River basin. The change in area ratio was obtained in each grid (0.5°). (d) The change of croplands area on Loess Plateau from 1990 to 2014 which got from statistical data. The 1980S represents the average value from 1980 to 1989.

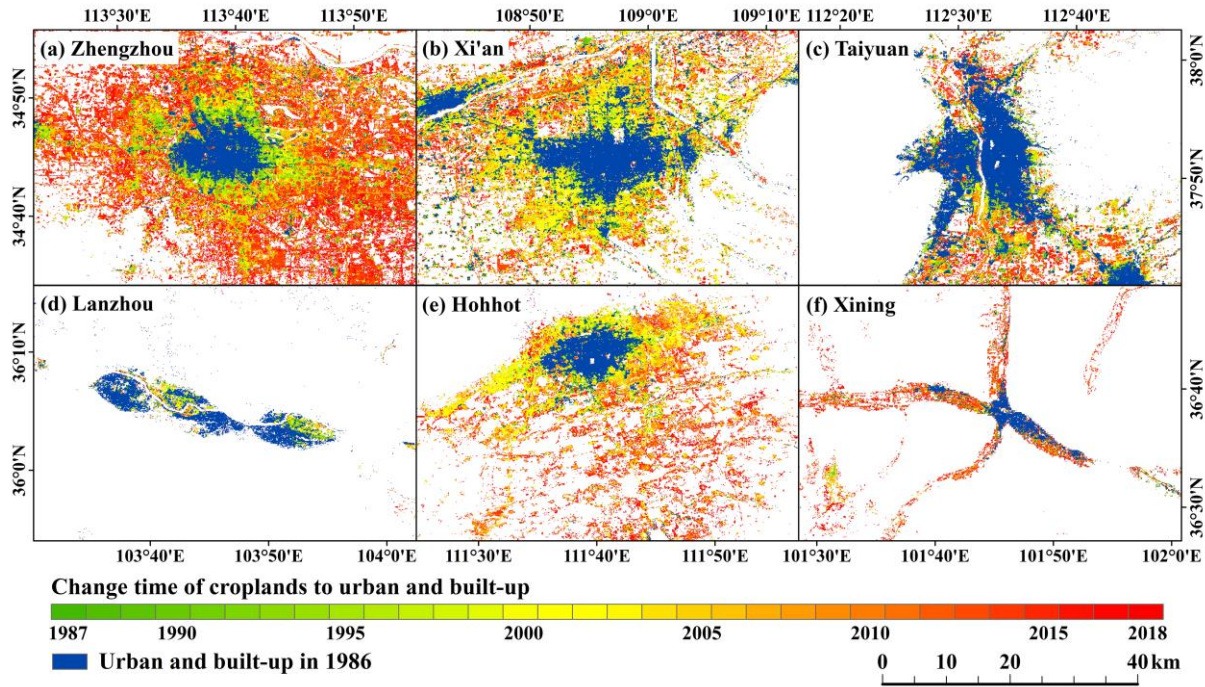


Figure S16. Geographical distribution of croplands to urban and built-up in six major cities of Yellow River basin: (a) Zhengzhou, (b) Xi'an, (c) Taiyuan, (d) Lanzhou, (e) Hohhot, and (f) Xining.

Table S1 Land use/cover and land use data used in related studies on the Yellow River basin. The Cbers denotes China-Brazil Earth Resources Satellite.

Study topic	Periods	Spatial resolution	Data source	Study area	Reference
Nutrient pollution	1977, 1996, 2000, and 2006	30 m	Landsat	Part of the Yellow River basin	[1]
Land use/cover change	1990, 1995, and 2000	30 m	Landsat	Yellow River basin	[2]
Soil erosion	2000 and 2008	30 m	Landsat, CBERS-2b	Loess Plateau	[3]
Ecosystem services	2000 and 2008	30 m	Landsat, CBERS-2b	Loess Plateau	[4]
Land use/cover change	1978, 1990, 1995, 2000, 2005, and 2010	30 m	Landsat	Part of the Loess Plateau	[5]
Ecosystem services	2000 and 2008	30 m	Landsat	Loess Plateau	[6]
Ecosystem services	1975, 1990, 2000, and 2008	30 m	Landsat, Cbers	Loess Plateau	[7]
Land use/cover change	1995, 2004, and 2010	30 m	Landsat	Part of the Yellow River basin	[8]
Land use/cover change	2001-2009 (yearly)	500 m	MODIS	Loess Plateau	[9]
Soil erosion	2000 and 2005	30 m	Landsat	Loess Plateau	[10]
Vegetation change	2010	250 m	MODIS	Yellow River basin	[11]
Soil erosion	1987, 1995, and 2007	30 m	Landsat	Part of the Loess Plateau	[12]
Vegetation restoration and water scarcity	2000 and 2008	Not specified	Landsat	Loess Plateau	[13]
Water scarcity and food scarcity	2010	Not specified	Not specified	Yellow River basin	[14]
Ecosystem carrying capacity	1990, 2000, 2008, and 2010	250 m	Landsat; CBERS-2b	Loess Plateau	[15]

Table S2 The accuracy of different band combinations. The values in the table represent the F1-score (the weighted harmonic mean of the producer's and user's accuracy) of each classifier in each class. Orange represents the corresponding classifier is better than the classifier with only using Landsat 6 spectral bands and blue represents the opposite case. The bands marked by * are the band combination for final classification. Aspect, landforms, Continuous Heat-Insulation Load Index (CHILI), and Multi-Scale Topographic Position Index (mTPI) are calculated from SRTM data [16]. Enhanced Vegetation Index (EVI) [17], Green Chlorophyll Vegetation Index (GCVI) [18], and Atmospherically Resistant Vegetation Index (ARVI) [19] are calculated from Landsat bands.

Bands	DBF	ENF	MF	Shrub	LCG	MCG	HCG	Crop	OT	UB	Water	Wet	Snow	DB	LV	Accuracy
*6 spectral bands	0.72	0.41	0.69	0.05	0.84	0.69	0.83	0.68	0.62	0.84	1.00	0.88	0.97	0.97	0.50	0.783
*Elevation + 6 bands	0.78	0.42	0.74	0.25	0.93	0.81	0.99	0.83	0.77	0.88	1.00	0.97	1.00	0.98	0.85	0.858
*NDVI+ NDVI_max + NDVI_min + 6 bands	0.80	0.67	0.74	0.17	0.88	0.79	0.89	0.89	0.74	0.87	1.00	0.92	0.98	0.99	0.59	0.840
*Topographic Diversity + 6 bands	0.72	0.45	0.70	0.02	0.87	0.75	0.86	0.79	0.72	0.93	1.00	0.99	0.99	0.96	0.52	0.804
*Slope + 6 bands	0.72	0.41	0.69	0.03	0.83	0.73	0.84	0.77	0.69	0.90	1.00	0.96	0.99	0.96	0.37	0.792
*NDBI + 6 bands	0.73	0.42	0.69	0.05	0.84	0.71	0.84	0.68	0.62	0.84	0.99	0.90	0.97	0.97	0.53	0.789
*NDMI + 6 bands	0.71	0.38	0.70	0.07	0.85	0.69	0.83	0.70	0.59	0.83	0.99	0.90	0.98	0.97	0.50	0.785
*SAVI + 6 bands	0.72	0.48	0.68	0.05	0.82	0.69	0.83	0.72	0.61	0.84	0.99	0.89	0.98	0.97	0.46	0.785
EVI + 6 bands	0.73	0.43	0.68	0.05	0.83	0.70	0.83	0.71	0.60	0.84	0.99	0.88	0.98	0.97	0.47	0.784
CHILI + 6 bands	0.72	0.41	0.69	0.07	0.86	0.66	0.83	0.68	0.64	0.85	1.00	0.90	0.99	0.96	0.56	0.784
Aspect + 6 bands	0.73	0.42	0.68	0.07	0.83	0.68	0.85	0.71	0.60	0.83	0.99	0.88	0.98	0.96	0.43	0.783
mTPI + 6 bands	0.72	0.45	0.68	0.05	0.82	0.69	0.84	0.69	0.64	0.85	0.99	0.89	0.98	0.96	0.47	0.782
Landforms + 6 bands	0.72	0.44	0.69	0.05	0.82	0.68	0.83	0.71	0.63	0.83	1.00	0.86	0.98	0.96	0.51	0.780
NDVI + 6 bands	0.73	0.37	0.69	0.05	0.81	0.67	0.82	0.61	0.64	0.82	0.99	0.90	0.98	0.97	0.51	0.780
GCVI + 6 bands	0.71	0.21	0.69	0.03	0.83	0.68	0.83	0.68	0.62	0.83	0.99	0.88	0.98	0.97	0.45	0.780
ARVI + 6 bands	0.71	0.39	0.68	0.04	0.83	0.69	0.83	0.70	0.58	0.82	1.00	0.89	0.98	0.96	0.42	0.778
MNDWI + 6 bands	0.72	0.33	0.69	0.05	0.82	0.66	0.83	0.67	0.62	0.84	0.99	0.89	0.98	0.97	0.38	0.778

Table S3 Confusion matrix of validation for test classifier in 2010. The overall accuracy is 90% and the Kappa coefficient is 0.89. UA denotes user's accuracy, PA denotes producer's accuracy, and bold numbers represent correctly classified ones.

	Prediction																
Class	DBF	ENF	MF	Shrub	LCG	MCG	HCG	Crop	OT	UB	Water	Wet	Snow	DB	LV	PA	
Reference	DBF	24021	3	2633	369	0	5	0	2	77	0	0	0	0	0	88%	
	ENF	6	879	748	0	0	0	0	0	1	0	0	0	0	0	54%	
	MF	4496	250	18380	555	0	3	24	3	61	0	0	0	0	0	77%	
	Shrub	1421	3	1073	1243	0	0	0	0	30	0	0	0	0	0	33%	
	LCG	0	0	0	0	11258	216	0	7	2	5	0	0	0	28	37	97%
	MCG	0	0	0	0	263	6088	0	1	5	0	0	0	0	47	103	94%
	HCG	2	0	39	0	0	0	12888	2	0	0	0	0	0	0	3	100%
	Crop	1	0	1	0	16	5	0	4047	22	29	0	0	0	0	6	98%
	OT	47	3	114	97	2	7	0	6	2945	5	1	0	0	0	0	91%
	UB	0	0	0	0	12	14	8	34	6	3596	3	0	0	4	15	97%
	Water	0	3	0	0	0	1	0	1	5	6	12573	0	0	0	1	100%
	Wet	0	0	0	0	0	0	0	3	0	10	7	2398	0	0	0	99%
	Snow	0	0	0	0	0	0	4	0	0	0	0	2383	2	0	0	100%
	DB	0	0	0	0	83	49	1	0	0	2	0	0	0	19645	65	99%
	LV	1	0	0	0	85	81	0	6	1	8	2	2	0	43	4613	95%
UA		80%	77%	80%	55%	96%	94%	100%	98%	93%	98%	100%	100%	100%	99%	95%	

Table S4 Test results for different classification methods.

Classification method	Training accuracy of the classifier	Kappa coefficient
CART	0.7998	0.7711
Random Forest	0.7983	0.7708
Linear Regression	0.7402	0.7026
Fast Naive Bayes	0.6423	0.6017
Continuous Naive Bayes	0.5985	0.5465
Minimum Distance	0.4950	0.4470

Table S5 Land use/cover datasets for comparison.

Dataset	Periods	Spatial resolution	Data source	Dataset provider
YR-LUC	1986-2018 Yearly	90 m	Landsat	This study
GLASS-GLC	1982-2015 Yearly	5 km	AVHRR	Liu, et al. [20]
MCD12Q1- V6	2001-2016 Yearly	500 m	MODIS Terra and Aqua data	USGS [21]
FROM-GLC	2010, 2015, 2017	30 m	Landsat	Gong, et al. [22]
GlobeLand30	2000, 2010	30 m	Landsat	National Geomatics Center of China [23]
GlobCover	2005, 2009	300 m	MERIS	European Space Agency [24]
GLCC	1992	1 km	AVHRR	USGS [25]
CGLS-LC100	2015	100 m	PROBA-V	Copernicus [26]

Table S6 List of related land use/cover mapping articles.

Reference	Title	Study area	Source data	Method	Data produced	Resolution of data produced	Validation strategy	Validation samples
Zhao Yuanyuan, et al.2019	Long-Term Land Cover Dynamics (1986–2016) of Northeast China Derived from a Multi-Temporal Landsat Archive	Northeast China	Landsat DEM	Random Forest	land cover mapping product	30m,1986-2016,Annual	equal-area stratified sampling	297 and 391 validation samples for the year 2000 and 2015
Kelley, et al.2018	Using Google Earth Engine to Map Complex Shade-Grown Coffee Landscapes in Northern Nicaragua	northwest Nicaragua	DEM Landsat 8	Random Forest machine learning algorithm	Complex Shade-Grown Coffee Landscapes Maps	30m,2014-2017,Seasonal	balanced training sampling	200 training points
Xiong, et al.2017	Automated cropland mapping of continental Africa using Google Earth Engine cloud computing	Africa	Sentinel-2 Landsat-8 SRTM 30 Slope	Random Forest; Support Vector Machines(SVM) Recursive Hierarchical Segmentation	a nominal 30-m cropland extent product	250m,2003-2014,16-day	Using GFSAD project Validation Dataset for validating	953 validation samples
Tsai, Yu; Stowi, et al.2018	Mapping Vegetation and Land Use Types in Fanjingshan National Nature Reserve Using Google Earth Engine	Fanjingshan National Nature Reserve	Landsat	Decision Tree (DT) Random Forest (RF)	vegetation and land use maps	30m,2010-2011,2015-2016,Seasonal	stratified by image illumination	128 points
Azzari, et al.2017	Landsat-based classification in the cloud: An opportunity for a paradigm shift in land cover monitoring	the Republic of Zambia	Landsat	Random Forest	a 30m-resolution cover map	30m,2011-2015,Seasonal	random and stratified sampling	12600 ground points
Hao, et al.2019	Land Use Change and Climate Variation in the Three Gorges Reservoir Catchment from 2000 to 2015 Based on the Google Earth Engine	the Three Gorges Reservoir Catchment	GlobeLand 30m Landsat DEM MODIS (LST, NDVI) GLDAS-2.1	Classification and Regression Tree (CART)	land use maps	30m,2000-2015,Annual	manually interpreted	1064 validation samples
Nyland,et al.2018	Land Cover Change in the Lower Yenisei River Using Dense Stacking of Landsat Imagery in Google Earth Engine	the Lower Yenisei River	Landsat	Random Forest	land cover maps	30m,1985-2017,Annual	verified by ground validation and primary knowledge of conditions	sample points were produced from an additional set of user-

								defined polygons separate from the classification algorithm
Zurqani, et al.2017	Geospatial analysis of land use change in the Savannah River Basin using Google Earth Engine	the Savannah River Basin	Digital Elevation Model (DEM) National Land Cover Database (NLCD) Landsat	Random Forest classifier algorithm	land cover classification maps	30m,1999-2015,Annual	using the validation dataset to validate	330 reference points
Aneece,et al.2018	Accuracies Achieved in Classifying Five Leading World Crop Types and their Growth stages Using Optimal Earth Observing-1 Hyperion Hyperspectral Narrowbands on Google Earth Engine	USA	USDA CDL dataset	Support Vector Machines (SVM)	A Hyperspectral Imaging Spectral Library	30m,2008-2015,Annual	Random sampling	969 samples for validation
Yin,et al.2017	Land use and land cover change in Inner Mongolia - understanding the effects of China's re-vegetation programs	Inner Mongolia	CAS-2000, Landsat, SRTM DEM MODIS(VI NDVI EVI blue MIR NIR)	Random Forest classification Trajectory-based change detection approach recovery (LandTrendr) algorithm	land cover classification maps	250m,2000-2014,Annual	Stratified calibrating	1078 calibration samples
Liu, Gong, et al.2019	Annual dynamics of global land cover and its long-term changes from 1982 to 2015	Global	GLASS-GLC MODIS(NDVI LAI FAPAAR ET GPP BBE ABD WS A)	Random Forest	GLASS-GLC products	5km,1982-2015,Annual	Use the 30m resolution FROM-GLC_v2 to evaluate the 2015 LC mapping results	23459 test samples units

			GMTED2010					
Xu, et al.2020	Annual 30-m land use/land cover maps of China for 1980-2015 from the integration of AVHRR, MODIs and Landsat data using the BFAST algorithm	China	MODIS GIMMS	BFAST algorithm	An annual nominal 30 m LULC datasets	30m,1980-2015,Annually	Independent validating and the hexagon based equal-area stratified random sampling	12000 samples in Beijing and 35000 validation samples totally
Teluguntla, et al.2018	A 30-m Landsat-derived cropland extent product of Australia and China using random forest machine learning algorithm on Google Earth Engine cloud computing platform	China and Australia	Landsat	Random Forest machine-learning algorithm	A 30m Landsat-derived cropland extent product	30m,2013-2015,16-day	Independent validating	900 samples in Australia and 1972 samples in China
Xie, et al.2019	Using Landsat observations (1988-2017) and Google Earth Engine to detect vegetation cover changes in rangelands - A first step towards identifying degraded lands for conservation	rangelands in Queensland (QLD) Australia	Landsat	the DynamicReference Cover Method (DRCM)	a vegetation cover change map	30m,1988-2017,Seasonal	Independent validating	1500 records
Deines, et al.2019	Mapping three decades of annual irrigation across the Us High Plains	The High Plains Aquifer in the central United States	Landsat	Random Forest Classifier the Bayesian Updating of Land-Cover (BULC) algorithm	30 m irrigation map	30m,1984-2017,Annual	Stratified random sampling	12650 samples
Bey, et al.2020	Mapping smallholder and large-scale cropland dynamics with a flexible classification system and pixel-based composites in an emerging frontier of Mozambique	Zambezia province of Mozambique	Landsat (NDVI)	Random Forest algorithm	based-pixels composite images	30m,2006-2016,Annual	Random sampling	4357 samples
Ge, Hu, et al.2019	Mapping annual land use changes in China's poverty-	China's poverty-	Landsat 8 VIIRS	Bayesian Hierarchical Model	annual land use mapping results	30m,2013-2018,Annual	random sampling	6530 samples

	stricken areas from 2013 to 2018	stricken areas	Global 30 m					
Parente, et al.2019	Assessing the pasturelands and livestock dynamics in Brazil, from 1985 to 2017: A novel approach based on high spatial resolution imagery and Google Earth Engine cloud computing	Brazil pasturelands	Landsat(NDVI, NDWI, CAI)	Random Forest algorithm	the totality of the Brazilian pastures	30m,1985-2017 Annual	Vote sampling	at least 4100 samples
Bontemps S, et al.2013	Consistent global land cover maps for climate modelling communities: current achievements of the ESA's land cover CCI	Global	MERIS FR, MERIS RR and SPOT-VGT	Machine Learning Unsupervised classification algorithms	The CCI global land cover maps	100m,1998-2012,Annual	Uncertainty	Uncertainty
Buchhorn ,et al.2020	Copernicus Global Land Cover Layers—Collection 2	Copernicus	PROBA-V UTM	Random Forest	the CGLS-LC100 discrete map layer	100m	probability sampling	21,752 sampling locations
Alencar, et al.2020	Mapping Three Decades of Changes in the Brazilian Savanna Native Vegetation Using Landsat Data Processed in the Google Earth Engine Platform	The Brasilia n Cerrado	Landsat	Empirical decision tree classification scheme Statistical Decision Tree Classification	multi-temporal land cover maps	30m,1985-2017,Annual	statistical sampling	21,000 independent sampling points
Tassi and Vizzari 2020	Object-Oriented LULC Classification in Google Earth Engine Combining SNIC, GLCM, and Machine Learning Algorithms	the Trasime no Lake	Sentinel 2 Landsat 8 PlanetScope	SNIC GLCM Machine Learning Random Forest (RF) Support Vector Machine (SVM)	an object-oriented classification approach	Uncertainty	statistical sampling	450 validation Points
Friedl, et al. 2010	MODIS Collection 5 global land cover: Algorithm refinements and characterization of new datasets	Global	MODIS	MLCT algorithm Decision Tree (DT)	the Collection 5 MODIS Global Land Cover Type product	500m, Annual	stratified random sampling	1860 points
Sedano, Lisboa, et al. 2020	Monitoring intra and inter annual dynamics of forest degradation from charcoal production in Southern Africa with Sentinel – 2 imagery	Sub-Saharan Africa	Sentinel-2	Supervised classification	forest degradation extent maps	10m,2016-2019,Seasonal	random sampling	10,000 simulations of possible values

Hansen, Potapov, et al. 2013	High-resolution global maps of 21st-century forest cover change	Global	Landsat	Supervised classification	21st-century forest cover change maps	30m,2000-2012,Annual	Uncertainty	Uncertainty
Jin, Azzari et al. 2019	Smallholder maize area and yield mapping at national scales with Google Earth Engine	Kenya and Tanzania	Sentinel-1 Sentinel-2	Random Forest (RF)	10m resolution maps of cropland presence	10m,2015-2017,Seasonal	local approach to validate	sample points were made from local places
Oliphant, Thenkabail, et al. 2019	Mapping cropland extent of Southeast and Northeast Asia using multi-year time-series Landsat 30-m data using a random forest classifier on the Google Earth Engine Cloud	Southeast and Northeast Asian Countries (SNACs)	Landsat GDEM	a pixel-based random forest (RF) supervised machine learning algorithm	cropland extent products	30m,2013-2016, four time-periods	a balanced sampling approach	250 randomly distributed sampling locations
Pekel, Cottam, et al. 2016	High-resolution mapping of global surface water and its long-term changes	Global	Landsat	Expert systems	Global surface water dataset	30m,1984-2015,Annual	Random sampling	40,124 control points
Liu, Duan, et al. 2020	Observations of water transparency in China's lakes from space	China	MODIS DEM	a remote sensing algorithm	a new algorithm for quickly mapping SDDs	500m,2000-2018,Annual	using the in-situ SDDs to validate	2236 samples
Liu, Hu et al. 2018	High-resolution multi-temporal mapping of global urban land using Landsat images based on the Google Earth Engine Platform	Global urban land	Landsat	Normalized Urban Areas Composite Index (NUACI)	new multi-temporal global urban land data	30m,1990-2010, five-year interval	stratified random sampling design	150 sample blocks
Liu, Huang, et al. 2020	High-spatiotemporal-resolution mapping of global urban change from 1985 to 2015	Global	Landsat	normalized urban areas composite index (NUACI) temporal segmentation approach	global annual urban extent dataset	30m,1985-2015,Annual	a multi-stage validation approach	500 validation samples
Li, Gong, et al. 2015	A 30-year (1984–2013) record of annual urban dynamics of Beijing City derived from Landsat data	Beijing	Landsat	a temporal consistency check and label modification scheme	urban-land sequences	30m,1984-2013,Annual	independent assessments	100 sample units

References

1. Ouyang, W.; Skidmore, A.K.; Toxopeus, A.G.; Hao, F.H. Long-term vegetation landscape pattern with non-point source nutrient pollution in upper stream of Yellow River basin. *J. Hydrol.* **2010**, *389*, 373-380, doi:10.1016/j.jhydrol.2010.06.020.
2. Wang, S.Y.; Liu, J.S.; Ma, T.B. Dynamics and changes in spatial patterns of land use in Yellow River Basin, China. *Land Use Pol.* **2010**, *27*, 313-323, doi:10.1016/j.landusepol.2009.04.002.
3. Fu, B.J.; Liu, Y.; Lu, Y.H.; He, C.S.; Zeng, Y.; Wu, B.F. Assessing the soil erosion control service of ecosystems change in the Loess Plateau of China. *Ecol. Complex.* **2011**, *8*, 284-293, doi:10.1016/j.ecocom.2011.07.003.
4. Lu, Y.; Fu, B.; Feng, X.; Zeng, Y.; Liu, Y.; Chang, R.; Sun, G.; Wu, B. A policy-driven large scale ecological restoration: quantifying ecosystem services changes in the Loess Plateau of China. *PLoS One* **2012**, *7*, e31782, doi:10.1371/journal.pone.0031782.
5. Zhou, D.C.; Zhao, S.Q.; Zhu, C. The Grain for Green Project induced land cover change in the Loess Plateau: A case study with Ansai County, Shanxi Province, China. *Ecol. Indicators* **2012**, *23*, 88-94, doi:10.1016/j.ecolind.2012.03.021.
6. Feng, X.; Fu, B.; Lu, N.; Zeng, Y.; Wu, B. How ecological restoration alters ecosystem services: an analysis of carbon sequestration in China's Loess Plateau. *Sci. Rep.* **2013**, *3*, 2846, doi:10.1038/srep02846.
7. Su, C.; Fu, B. Evolution of ecosystem services in the Chinese Loess Plateau under climatic and land use changes. *Global Planet. Change* **2013**, *101*, 119-128, doi:10.1016/j.gloplacha.2012.12.014.
8. Ottinger, M.; Kuenzer, C.; Liu, G.; Wang, S.; Dech, S. Monitoring land cover dynamics in the Yellow River Delta from 1995 to 2010 based on Landsat 5 TM. *Appl. Geogr.* **2013**, *44*, 53-68, doi:10.1016/j.apgeog.2013.07.003.
9. Fan, X.; Ma, Z.; Yang, Q.; Han, Y.; Mahmood, R.; Zheng, Z. Land use/land cover changes and regional climate over the Loess Plateau during 2001–2009. Part I: observational evidence. *Clim. Change* **2014**, *129*, 427-440, doi:10.1007/s10584-014-1069-4.
10. Sun, W.Y.; Shao, Q.Q.; Liu, J.Y.; Zhai, J. Assessing the effects of land use and topography on soil erosion on the Loess Plateau in China. *Catena* **2014**, *121*, 151-163, doi:10.1016/j.catena.2014.05.009.

11. Jiang, W.G.; Yuan, L.H.; Wang, W.J.; Cao, R.; Zhang, Y.F.; Shen, W.M. Spatio-temporal analysis of vegetation variation in the Yellow River Basin. *Ecol. Indicators* **2015**, *51*, 117-126, doi:10.1016/j.ecolind.2014.07.031.
12. Chen, N.; Ma, T.Y.; Zhang, X.P. Responses of soil erosion processes to land cover changes in the Loess Plateau of China: A case study on the Beiluo River basin. *Catena* **2016**, *136*, 118-127, doi:10.1016/j.catena.2015.02.022.
13. Feng, X.; Fu, B.; Piao, S.; Wang, S.; Ciais, P.; Zeng, Z.; Lü, Y.; Zeng, Y.; Li, Y.; Jiang, X., et al. Revegetation in China's Loess Plateau is approaching sustainable water resource limits. *Nat. Clim. Chang.* **2016**, *6*, 1019-1022, doi:10.1038/nclimate3092.
14. Yin, Y.Y.; Tang, Q.H.; Liu, X.C.; Zhang, X.J. Water scarcity under various socio-economic pathways and its potential effects on food production in the Yellow River basin. *Hydrol. Earth Syst. Sci.* **2017**, *21*, 791-804, doi:10.5194/hess-21-791-2017.
15. Liang, W.; Fu, B.; Wang, S.; Zhang, W.; Jin, Z.; Feng, X.; Yan, J.; Liu, Y.; Zhou, S. Quantification of the ecosystem carrying capacity on China's Loess Plateau. *Ecol. Indicators* **2019**, *101*, 192-202, doi:10.1016/j.ecolind.2019.01.020.
16. Theobald, D.M.; Harrison-Atlas, D.; Monahan, W.B.; Albano, C.M. Ecologically-Relevant Maps of Landforms and Physiographic Diversity for Climate Adaptation Planning. *PLoS One* **2015**, *10*, e0143619, doi:10.1371/journal.pone.0143619.
17. Huete, A.; Didan, K.; Miura, T.; Rodriguez, E.P.; Gao, X.; Ferreira, L.G. Overview of the radiometric and biophysical performance of the MODIS vegetation indices. *Remote Sens. Environ.* **2002**, *83*, 195-213, doi:10.1016/s0034-4257(02)00096-2.
18. Gitelson, A.A.; Vina, A.; Arkebauer, T.J.; Rundquist, D.C.; Keydan, G.; Leavitt, B. Remote estimation of leaf area index and green leaf biomass in maize canopies. *Geophys. Res. Lett.* **2003**, *30*, 1248, doi:10.1029/2002gl016450.
19. Kaufman, Y.J.; Tanre, D. Atmospherically resistant vegetation index (ARVI) for EOS-MODIS. *IEEE Trans. Geosci. Remote Sensing* **1992**, *30*, 261-270, doi:10.1109/36.134076.
20. Liu, H.; Gong, P.; Wang, J.; Clinton, N.; Bai, Y.; Liang, S. Annual dynamics of global land cover and its long-term changes from 1982 to 2015. *Earth Syst. Sci. Data* **2020**, *12*, 1217-1243, doi:10.5194/essd-12-1217-2020.
21. Friedl, M.A.; Sulla-Menashe, D.; Tan, B.; Schneider, A.; Ramankutty, N.; Sibley, A.; Huang, X. MODIS Collection 5 global land cover: Algorithm refinements and characterization of new datasets. *Remote Sens. Environ.* **2010**, *114*, 168-182, doi:10.1016/j.rse.2009.08.016.

22. Gong, P.; Wang, J.; Yu, L.; Zhao, Y.; Zhao, Y.; Liang, L.; Niu, Z.; Huang, X.; Fu, H.; Liu, S., et al. Finer resolution observation and monitoring of global land cover: first mapping results with Landsat TM and ETM+ data. *Int. J. Remote Sens.* **2012**, *34*, 2607–2654, doi:10.1080/01431161.2012.748992.
23. Jun, C.; Ban, Y.; Li, S. China: Open access to Earth land-cover map. *Nature* **2014**, *514*, 434, doi:10.1038/514434c.
24. Bontemps, S.; Defourny, P.; Radoux, J.; Van Bogaert, E.; Lamarche, C.; Achard, F.; Mayaux, P.; Boettcher, M.; Brockmann, C.; Kirches, G. Consistent global land cover maps for climate modelling communities: current achievements of the ESA's land cover CCI. In Proceedings of ESA Living Planet Symposium, Edinburgh; pp. 9–13.
25. Loveland, T.R.; Reed, B.C.; Brown, J.F.; Ohlen, D.O.; Zhu, Z.; Yang, L.; Merchant, J.W. Development of a global land cover characteristics database and IGBP DISCover from 1 km AVHRR data. *Int. J. Remote Sens.* **2010**, *21*, 1303–1330, doi:10.1080/014311600210191.
26. Buchhorn, M.; Smets, B.; Bertels, L.; Lesiv, M.; Tseddbazar, N.; Herold, M.; Fritz, S. Copernicus Global Land Service: Land Cover 100m: Epoch 2015: Globe. *Version V2.0.2* **2019**, 10.5281/zenodo.3243509, doi:10.5281/zenodo.3243509.